Localization with Cellular Signal RSRP Fingerprint of Multiband and Multicell

Zhinan Hu, Xin Chen, *Senior Member, IEEE*, Zhenyu Zhou, *Senior Member, IEEE*, and Shahid Mumtaz, *Senior Member, IEEE*

***Abstract*—Precisely predicting the location of the user in a Global-Navigation-Satellite-System-degraded environment is a highly challenging task. Localization based on cellular signal fingerprints is one of the promising solutions to this problem and has attracted increasing attention. Long Term Evolution (LTE) signal is popularly utilized for localization due to its global usage, extensive urban coverage, and favorable signal properties. This paper proposes a new multiband multicell Reference Signal Received Power (MBMC-R) fingerprint, which properly fuses LTE signals' carrier band information, the physical cell identifier information, and RSRP values. Next, a sequential block-matching weight K nearest neighbor algorithm with a cosine similarity criterion is specially designed for performing the pattern-matching localization with the MBMC-R fingerprint. The proposed method also includes the derivation of the Cramer-Rao lower bound, which reveals the impact of various factors on the lower bound of position error. Simulation and on-field experiments prove the performance superiority over other fingerprint localization algorithms reported in the literature.**

***Index Terms*—fingerprint location, LTE signal, CRLB, sequential matching, WKNN.**

I. Introduction

In recent years, location-based services have become increasingly important in various applications. Although Global Navigation Satellite Systems (GNSS) can achieve satisfactory localization precisions in many outdoor scenarios, it still suffers from severe performance degradations or fix failures in dense urban environments [1], such as narrow urban canyons, tunnel, and electromagnetic interference environments. Therefore, many wireless signals, such as Frequency Modulation (FM), Digital Television (DTV), Long Term Evolution (LTE), the 5th Generation Mobile Communication Technology (5G), Wireless Fidelity (WiFi), Ultra-wideband (UWB), and Bluetooth, are utilized for localization as a complement to GNSS [2]. These techniques typically adopt the trilateration principle to perform localization with measurements from multiple transmitter nodes [3]. The measurements may include the time-of-arrival (TOA) [4], [5], the time-difference of arrival (TDOA) [6], the angle of arrival (AOA) [7], or the received signal strength (RSS) [8]. However, these localization techniques are normally susceptible to multipath or non-line-of-sight signals and require precise timing synchronization among transmitter nodes [9].

Another approach for wireless localization is based on the principle of fingerprint matching. This type of method needs to create a database of fingerprints by measuring a certain signal fingerprint that normally contains a close relationship with the position information. During the online localization phase, a pattern-matching method is often utilized to estimate the unknown user positions with the known fingerprint database.

Traditionally, the RSS value is mainly adopted for forming the fingerprint database due to its computational simplicity [10]. However, the inconsistency and non-standardization of the RSS fingerprint among different user devices will lead to large positioning errors. Therefore, differential RSS (DRSS) is further proposed to increase the signature robustness [11], [12]. The multipath channel state information (CSI) contains abundant information about the local wireless propagation environment of the user, making it a valuable fingerprint for localization [13]–[15]. This type of fingerprint is less susceptible to signal fluctuations than the RSS/DRSS fingerprint in multipath environments.

It is still found that the localization with a single type of fingerprint is quite sensitive to environmental variations. If more types of fingerprints can be jointly used, it will naturally enhance the localization accuracy and robustness. In [16], the DRSS and the hyperbolic location fingerprints are combined to leverage the mutually complementary features. In [17], Peng et al. proposed a joint fingerprint that is composed of the RSS indication (RSSI) and the phase difference of arrival (PDOA). Guo et al. combined RSS, power spectral density, covariance matrix, signal subspace, fourth-order cumulant, and fractional low-order moment of the received signals to form a compound fingerprint for localization [18]. The fusion of RSS and CSI fingerprints was frequently employed by researchers, although they contain abundant signal strength information [19], [20]. Tao et al. proposed the combination of the RSS and AOA as a joint fingerprint [21]. Generally speaking, the fusion of the RSS with the AOA/TOA/CSI information is typically adopted in the literature.

As the cellular signal communication system evolves and progresses, the LTE system has covered most of the cities and villages around the world, and the utilization of mid-

Manuscript received 13 November 2023; revised 19 March 2024; accepted 18 April 2024. This work is part of the 6G-SENSES project from the Smart Networks and Services Joint Undertaking (SNS JU) under the European Union's Horizon Europe research and innovation programme under Grant Agreement No 101139282.(*Corresponding author: Xin Chen.*)

Zhinan Hu and Xin Chen are with School of Electronic Information and Electrical Engineering, Shanghai Jiao Tong University, Shanghai 200240, China.(e-mail: huzhinan_21@sjtu.edu.cn; xin.chen@sjtu.edu.cn).

Zhenyu Zhou is with the State Key Laboratory of Alternate Electrical Power System with Renewable Energy Sources, North China Electric Power University, Beijing, 102206, China.(e-mail: zhenyu_zhou@ncepu.edu.cn)

Shahid Mumtaz is with Department of Applied Informatics Silesian University of Technology Akademicka 16 44-100 Gliwice, Poland and Nottingham Trent University, Departement of Computer Sciences.(e-mail: dr.shahid.mumtaz@ieee.org)

band spectrum for 5G deployment is currently limited to approximately 25% of existing 4G sites worldwide [22]. With the advantages of broad coverage and high signal quality, the LTE system signal has become a promising candidate for localization, especially in the urban environment [23]. Furthermore, the study of LTE lays a solid foundation for future research on 5G technology. The LTE Reference Signal Received Power (RSRP) fingerprint is often used due to its easy access by the user terminals [24]. Besides, the CSI of the LTE signal is another popular candidate for fingerprint [25]. Hu et al. utilized the spectrum of the Zadoff-Chu sequence spectrum of the LTE signal as a fingerprint to alleviate the random fading noise [26]. Li et al. converted the original LTE signal measurements into a type of grayscale image fingerprint to reveal more details in the signal propagation information [27]. In [28], 1-dimensional (1D) RSSIs associated with LTE signal IDs, generated from a combination of a physical cell identifier (PCI) and E-UTRA absolute radio frequency channel number (EARFCN), were extracted to create the combined fingerprint. He et al [29] leveraged the TDOA measurements to estimate a rough approximation of the user's position and then employed the RSS fingerprint to obtain a more precise positioning estimation.

As to the online localization phase, the methods like the deterministic-model-based algorithms [30], the probabilistic-model-based algorithms [18], [20], and the machine-learning-based algorithms [31]–[39] are all widely used. Due to the significant progress in innovations in artificial intelligence in recent times, the machine-learning-based method has shown remarkable localization accuracy enhancement over other types of approaches. The K Nearest Neighbor (KNN) algorithm [31], [32], the Weight K Nearest Neighbor (WKNN) algorithm [33], [34], the Convolutional Neural Network (CNN) algorithm [35], [36], the Artificial Neural Network (ANN) algorithm [37], [38], and the Deep Neural Network (DNN) algorithm [39] are popular for the localization with fingerprints.

How to assess the effects of different types of fingerprints on positioning precision is another important research work. Jiseon et al. developed the Cramer-Rao lower bound (CRLB) of the positioning precision using the RSS fingerprint [40]. Gui et al. derived the localization accuracy CRLB with the CSI fingerprint for the indoor environment [41]. Jiang et al. analyzed the CRLB of localization errors with joint fingerprints, such as RSS/AOA, RSS/TOA, AOA/TOA, and AOA/RSS/TOA [42].

A. Motivations

Through the analysis of the current research status, it is found that most of the proposed fingerprint-based localization algorithms are aimed to work in the indoor environment. For the outdoor environment, the space dimensionality and the surrounding random objects are much larger and much more complex than that of the indoor environment. Thereby, the CSI fingerprint, which is frequently used for indoor localization, may not be a better choice because it is quite susceptible to the small variations of the surrounding environment. This susceptibility will make the localization performance unstable.

In contrast, the RSRP value is more robust against small-scale propagation channel changes for the outdoor environment [43]. Unfortunately, the conventional way of designing the RSRP fingerprint is just packing the RSRP values of signals transmitted from different base stations (BSs) into an array and leaving it in the pattern-matching algorithm. This format of the fingerprint abandons the underlying frequency and cell identifier information associated with the RSRP values. Thus, the localization precision with this format of the RSRP fingerprint is unsatisfactory.

The LTE network contains multiple BSs physically located at different positions. Each BS is divided into three sectors, and each sector corresponds to one PCI. According to the 3GPP standards of the LTE signal [44], to enhance the quality of communications, multiple cells operate at different frequencies cover the same sector, and a device can receive LTE signals from different cells simultaneously. Therefore, UE can receive different LTE signals at one position. The carrier bands and PCIs of all the observed LTE signals depend on the nearby BSs. Suppose all the observed RSRPs at a position are properly manipulated along with their corresponding carrier bands and PCI information. In that case, it can be expected that the new type of fingerprint will have a closer and unambiguous bond with its geometrical location. This advantage will naturally improve the localization performance.

Furthermore, with the introduction of the multi-bands and multi-cells information, it can be expected that the fingerprints of adjacent locations will have a certain similarity because nearby locations will receive the signals of most of the same BSs. However, the RSRP values will be different to a certain extent. This similarity property can be utilized in the pattern-matching algorithm to mitigate the localization error further.

B. Contributions

In this paper, a novel type of fingerprint, expressed as a 2-dimensional (2D) RSRP array, is designed. The row index of the array stands for all the carrier bands allocated to the BS transmitters by the service provider. The column index of the array stands for all PCIs defined by the 3GPP standards for the LTE signal. The RSRP values of the received LTE signals are padded in the array according to their corresponding band and cell PCI indices. If there is no received signal at a band or a PCI, a zero is filled into the corresponding position of the array. Therefore, this fingerprint looks more like a featured image than a vectorized datum. We name this design as multiband multicell RSRP (MBMC-R) fingerprint. The novel MBMC-R fingerprint design brings a few advantages over the traditional LTE signal's fingerprint schemes:

First, the proposed 2D MBMC-R fingerprint utilizes the multi-band and multi-cell RSRP information. Compared to the classical 1D RSS fingerprints constructed using multiple access points, the proposed fingerprint fully utilizes spatial and frequency diversity, enhancing the number of fingerprint features while providing a clearer and more detailed description of RSRP variations in spatial and frequency dimensions. The obtained MBMC-R fingerprint exhibits a clearer and closer relationship with the sampled position. It also mitigates

the instability caused by the small-scale variations in the propagation channel.

Second, the proposed sequential block-matching weight K nearest neighbor (SWKNN) algorithm fully leverages the features and advantages of MBMC-R fingerprints to achieve accurate online positioning. Sequential block-matching is adopted based on spatial continuity and frequency continuity 2D MBMC-R fingerprint. The cosine similarity criterion is well suited for 2-D and sparse MBMC-R fingerprints. It improves the similarity measurement method of the online matching positioning algorithm, thereby enhancing the accuracy and robustness of the matching. The WKNN method utilizes the fingerprint of the training dataset for matching, and it can adapt to different offline datasets. It adjusts the matching results with weights to effectively reduce the influence of noise and outliers, making the localization algorithm more robust.

Third, the CRLB bound for the MBMC-R fingerprint localization method is derived. The Fisher information matrix (FIM), which provides the lower bound of the variance of the location estimation, has been confirmed to be related to the number of carrier bands, the number of cells, and the location of BS and UE. It has also been demonstrated that the localization accuracy increases with the number of carrier bands and cells.

In addition, it is essential to emphasize that the proposed fingerprinting methods are not limited to specific types of cellular signals. This method can be applied to various cellular signals, such as GSM, 5G, etc. This versatility makes the proposed fingerprint localization methods more flexible and scalable in practical applications.

The structure of the remainder of this paper is outlined below: The system model is presented in Section II. In Section III, the design of the MBMC-R fingerprint is given. The SWKNN positioning algorithm is used in Section IV. Next, the CRLB of the proposed fingerprints is analyzed in Section V. Performance evaluation by simulations and experimental is presented in Section VI. Finally, Section VII provides the conclusion of the study.

II. System Model

With the broad deployment of the LTE system around the world, signal coverage in most places has reached quite a good status. Often, a UE at a position can receive the signals with different PCIs in different carrier bands that are transmitted from multiple BSs. For the purpose of communication, the UE will mainly connect with a single BS to get communication access. For the purpose of localization, all the signals received from different BSs can be simultaneously analyzed to obtain the most accurate estimation of the UE position. Fig. 1 illustrates this scenario.

A. LTE Signal Model

In the following, we consider that the LTE downlink signal uses Orthogonal Frequency Division Multiplexing (OFDM), normal Cyclic Prefix (CP) length, and one antenna port in one carrier band corresponding to center frequency. Without loss of generality, this analysis can be applied to other pilot cellular

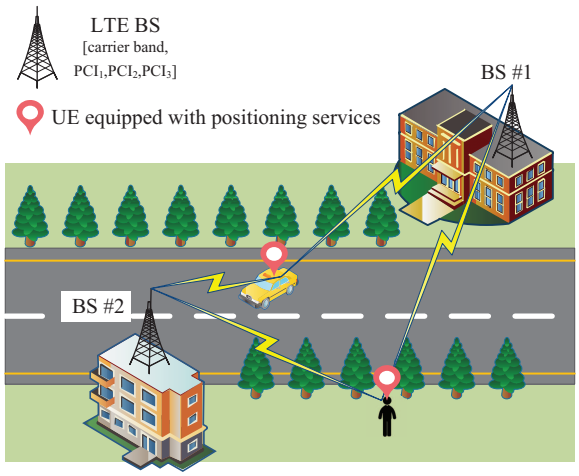

Fig. 1. Illustration for the multiple BS signals' observation at a position.

signals, such as 5G and future generations. In the OFDM system, the transmitted symbols that represent the smallest time intervals in the LTE frame are mapped to different subcarriers. The spacing of adjacent subcarriers is Δf. Assume that N_r subcarriers are assigned for data transmission. Then, zero-padding is used to extend N_r data symbols to N_c to reduce the interference in the received signal. Next, the CP is created by repeating the final N_{cp} elements of the symbol at its beginning, which helps mitigate interference caused by multipath propagation. Finally, the symbol sequence undergoes an inverse fast Fourier transform and is then up-converted to the carrier frequency for transmission.

On the UE side, all the received LTE signals are first down-converted and then sampled. Then, the cyclic prefix removal and the fast Fourier transform operation are applied to the digitized samples. Hence, the i_sth symbols received signal [4], [45] is expressed as

$$R_{i_s}(k) = e^{j\pi e_f} e^{j2\pi(i_s(N_c+N_{cp})+N_c)\frac{e_f}{N_c}} e^{je_\varphi} Y_{i_s}(k) H_{i_s}(k) + W_{i_s}(k), \quad (1)$$

where $k = 0, ..., N_c - 1$ is the subcarrier index, $e_f = \frac{f_D}{\Delta f}$, and f_D is the overall carrier frequency offset by summing up all the effects of Doppler frequency, clock drift, and oscillator mismatch. e_φ represents carrier phase errors normalized by the sampling interval T_s. $Y_{i_s}(k)$ denotes the frequency domain representation of the transmitted signals and $H_{i_s}(k)$ is the channel frequency response (CFR). $W_{i_s}(k) \in N(0, \sigma^2)$ signifies the sum of all interfering factors, including thermal noise and signals from adjacent cells, which follows a Gaussian distribution with zero mean and variance σ^2. It needs to be noted that the Doppler frequencies of different subcarriers vary slightly. However, this difference is very small and can be neglected in the following study.

In the LTE signal, the cell-specific reference signal (CRS) subcarrier is broadcast in every frame regardless of whether any data is transmitted to any UE. Hence, it is suitable to be used for positioning. CRS subcarriers are allocated based on the PCI and symbol number. The PCI serves as an identifier for the cell, numbered from 0 to 503. The way of decoding the PCI

number can be referred to [45]. In this study, the kth subcarrier and $i_{\rm s}$th symbol transmission CRS signal is represented as $S_{i_{\rm s}}(k)$, where $k = m_{\rm s}\Delta_{\rm CRS} + \kappa$ with $m_{\rm s} = 0, ..., M_{\rm s} - 1$ and $M_{\rm s}{=}\lfloor N_r/\Delta_{\rm CRS}\rfloor$. Here, $\Delta_{\rm CRS} = 6$ and $\kappa \in \{0, ..., 5\}$ is a constant shift determined by the PCI, transmission antenna port number and the symbol number $i_{\rm s}$.

As the CRS sequence is already known at the receiver after coarse symbol synchronization, the CFR estimation by utilizing the pilot CRS tones transmitted in symbol $i_{\rm s}$ can then be obtained as

$$\hat{H}_{i_{\rm s}}(k) = R_{i_{\rm s}}(k)S^*_{i_{\rm s}}(k) = e^{j\delta\theta_{i_{\rm s}}}H_{i_{\rm s}}[k] + {W_{i_{\rm s}}}'[k], \quad (2)$$

where $\delta\theta_{i_{\rm s}} = \pi e_f\left[N_c + 2(i_{\rm s}(N_c + N_{cp}) + N_{cp})\right]/N_c{+}e_\varphi$ denotes the average carrier phase error and ${W_{i_{\rm s}}}'(k){=}W_{i_{\rm s}}(k)S^*_{i_{\rm s}}(k)$.

Thus, the RSRP is calculated based on the vectors $\hat{H}_{i_{\rm s}}(k)$ as

$$\text{RSRP}_{i_{\rm s}}{=}\frac{1}{M_{\rm s}}\sum_{{\rm k}=0, k\in m_{\rm s}\Delta_{\rm CRS}+\kappa}^{N_c-1}\left|\hat{H}_{i_{\rm s}}(k)\right|^2. \quad (3)$$

B. LTE Signal Propagation Model

We consider that the RSRP value (in dBm) of the LTE signal with different carrier bands follows the simple log-distance radio propagation model as

$$P_{ik_m} = P_{0k_m} + L(f_c^m) + \beta_{k_m}\log d_{ik_m} + X_{\sigma_{f_c^m}}, \quad (4)$$

where P_{ik_m} is the RSRP with the distance d_{ik_m} between the ith location of UE and the k_mth BSs. P_{0k_m} denotes the transmission power of the k_mth BS. f_c^m denotes the center frequency corresponding to the mth carrier band. $L(f_c^m)$ represents the fading that corresponds to the mth carrier band. The path-loss exponent β_{k_m} is determined by the propagation conditions. $X_{\sigma_{f_c^m}}$ is a Gaussian random variable with a mean zero and a variance of $\sigma^2_{f_c^m}$.

Outdoor LTE signal transmission satisfies the Okumura model. Hence, there holds $\beta_{k_m} = 44.9 - 6.55\log h_{\rm kte}$, where $h_{\rm kte}$ represents the effective height of the k_mth BS antenna. The fading loss function $L(f_c^m)$ is expressed as

$$L(f_c^m){=}\begin{cases}46.3{+}33.9\log f_c^m{+}\psi{+}C_{\rm M}, 1.5{\rm GHz}{\le}f_c^m{\le}\,2{\rm GHz},\\ 69.55{+}26.16\log f_c^m{+}\psi, 150{\rm MHz}{\le}f_c^m{\le}\,1.5{\rm GHz},\end{cases} \quad (5)$$

where $C_{\rm M}$ denotes the metropolitan center calibration factor, and ψ is computed as

$$\psi = -13.82\log h_{\rm te} - \alpha(h_{\rm re}) + C_{\rm cell} + C_{\rm terrain}, \quad (6)$$

where $h_{\rm re}$ stands for the effective height of the UE. $\alpha(h_{\rm re})$ represents the effective antenna correction factor. $C_{\rm cell}$ is the cell type correction factor. $C_{\rm terrain}$ is a topographic calibration factor.

III. Design of Multiband and Multicell RSRP Fingerprint

The traditional RSRP fingerprint design methods use a vectorized format to contain all the RSRP values of the signals transmitted from different BSs [10], [28]. This type of fingerprint format ignores the PCI and carrier band information associated with the LTE signals. Actually, different BSs have different PCIs and carrier bands. Properly incorporating these two types of information will naturally enhance the differentiability between the fingerprints of different locations, which, in turn, will improve localization accuracy.

To solve the aforementioned problem, a 2D RSRP array fingerprint is designed. The row indices of the array represent the carrier bands that are allocated to the BS transmitters by the service provider, and the column indices are the PCI values defined by the 3GPP standards. In each cell of the array, the RSRP value of the signal for the corresponding carrier band and PCI is filled. Therefore, the proposed MBMC-R fingerprint is expressed as

$$F{\rm in}^{p_i} = \left\{\begin{array}{c}\text{RSRP}^{p_i}_{1,\text{PCI}_1}\cdots\text{RSRP}^{p_i}_{1,\text{PCI}_N}\\ \vdots\ddots\vdots\\ \text{RSRP}^{p_i}_{M_f,\text{PCI}_1}\cdots\text{RSRP}^{p_i}_{M_f,\text{PCI}_N}\end{array}\right\}, \quad (7)$$

where $p_i = (x_i, y_i)$ stands for the location at which the MBMC-R fingerprint is collected, M_f denotes the number of carrier bands occupied by the LTE signals in the area, and N is the number of PCIs.

It needs to be pointed out that the PCI values range from 0 to 503, as defined by the standards, while the range of carrier bands, as well as the center frequency of each band, is decided by the local wireless service provider. Therefore, the occupied carrier band information for the local area needs to be investigated in advance.

The RSRP value ranges from -140dBm to -44dBm according to the 3GPP regulations [46]. The value of -140dBm indicates a very weak signal strength, while the value of -44dBm indicates a very strong one. If the RSRP value of the received signal is lower than -140dBm or there is no signal for the cell of a combination of a carrier band and a PCI number, a NULL_0 flag is filled correspondingly, which stands for an absolute zero value. It is defined as the purpose of conveniently utilizing the cosine similarity criteria in the localization algorithm. If we use $F{\rm in}^{p_i}_{m,\text{PCI}_n}$ to denote the value of the cell (m, PCI_n) in the MBMC-R fingerprint array $F{\rm in}^{p_i}$, it has

$$F{\rm in}^{p_i}_{m,\text{PCI}_n}{=}\left\{\begin{array}{c}\text{RSRP}_{m,\text{PCI}_n}, \text{if RSRP} \ge -140\text{dBm},\\ \text{NULL}_0, \text{if RSRP} < -140\text{dBm},\end{array}\right. \quad (8)$$

where $m \in [1, M_f]$ represents the mth carrier band index, and $\text{PCI}_n \in [1, N]$ denotes the nth PCI index.

Fig. 2 illustrates an example of the MBMC-R fingerprint. In this example, the MBMC-R fingerprint is shown as a grayscale image for an easier illustration. The size of the image is $M_f \times N$, which is equivalent to the size of the fingerprint array. Each pixel in the image is equivalent to the cell of the array. The brightness of a pixel depends on the value of the RSRP for that cell. The brighter the pixel, the higher the RSRP. It is readily seen that the MBMC-R fingerprint is typically sparse.

Fig. 3 shows the results of obtaining the RSRP by Universal Software Radio Peripheral (USRP) on the campus of Shanghai Jiao Tong University at different times. The center frequency of the LTE signal is 2145 MHz. The RSRP with different

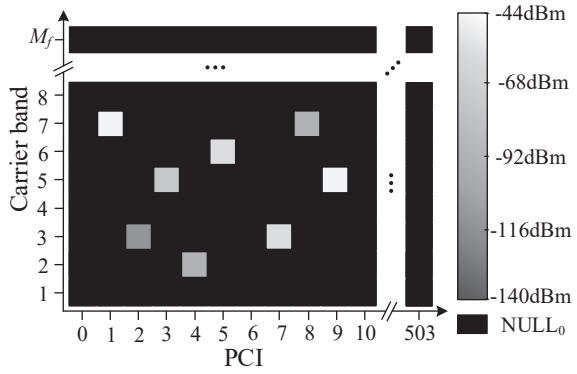

Fig. 2. Illustration for the MBMC-R fingerprint.

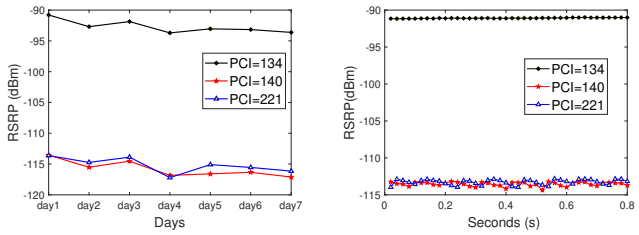

(a) (b)

Fig. 3. Illustration of RSRP results for different PCIs. (a) RSRP results versus days. (b) RSRP results versus seconds.

PCI values remains relatively stable over time, indicating the time-stability of the proposed MBMC-R fingerprint.

Remark 1. *Here, it is noted that offline fingerprints possess temporal stability and spatial relevance. Consequently, the fingerprint database does not need frequent updates. The fingerprint database only needs updating when the surrounding infrastructures or the positions of transmitting signal BSs significantly change. Furthermore, database filling can be achieved through interpolation and matrix prediction methods, facilitating the establishment of large-size fingerprint datasets.*

IV. SWKNN Localization Algorithm Based on MBMC-R Fingerprints

The fingerprint-based localization method typically comprises two principal steps: The first is the offline phase, in which the fingerprints are sampled at reference positions within the application area. The second is the online phase, in which the real-time localization is performed based on the established fingerprint database. An offline dataset is constructed with MBMC-R fingerprints measured at reference points (RP), i.e., points with measured coordinates. In the online phase, UE's MBMC-R fingerprint is compared with those in the offline database to determine the location. Only devices capable of measuring MBMC-R fingerprints are needed during the online localization phase, such as smartphones or USRPs. Fig. 4 illustrates the workflow of the MBMC-R fingerprint localization algorithm.

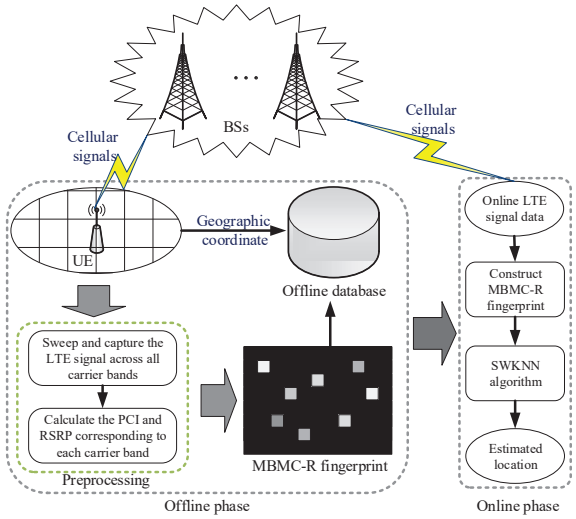

Fig. 4. Overall MBMC-R fingerprint localization architecture.

A. Offline Fingerprint Construction

First, all the carrier bands that are utilized by the BSs in the target application area need to be investigated. The number of the carrier bands and their center frequencies determine the row size M_f and the indices of the MCMB-R fingerprint array. The indices of the column of the array always span from 0 to 503 according to the definition given in Section III.

Next, evenly divide the target area into small grids. UE sweeps the LTE signal across all the carrier bands at an offline grid point. The PCIs and RSRPs of all observed LTE signals are computed. Then, the MBMC-R fingerprint for a grid point can be obtained. The coordinates of the grid points are recorded as the location information associated with this fingerprint. Repeat the above process for all grid points in the target area, and the entire MBMC-R fingerprint database can be established.

B. Online SWKNN Localization Algorithm

Many fingerprint localization algorithms have been proposed in the past decade [18], [20], [30]–[35], [38], [39]. Plenty of matching time is essentially required for the online matching phase of the neural networks, increasing the implementation complexity of the localization method. During these two relatively extended processes, it is possible that the environment undergoes alterations, rendering the measurements collected for online positioning phase obsolete [47]. In the small size of the offline training database, WKNN can realize quick and robust localization. This section introduces the method for constructing offline fingerprints and formulates the online fingerprint SWKNN matching methodology.

It has been known that MBMC-R fingerprint given in (7) has a sparse property. According to the propagation model in (4), it can be predicted that the MBMC-R fingerprints between adjacent positions also have a spatial correlation property. This is because the RSS changes with the distance of the UE to the transmitting BS. According to (4), if we ignore the effect of the random term $X_{\sigma_{f_c^m}}$, the P_{ik_m} will be a continuous function about d_{ik_m}, which means that the RSRPs at nearby positions

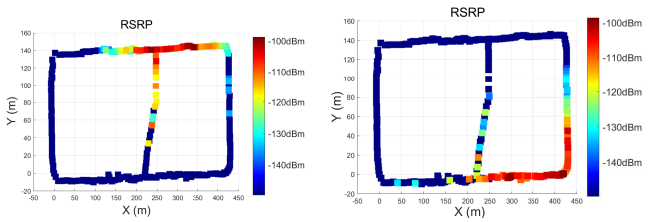

(a) f_c^m = 2145MHz, PCI = 134. (b) f_c^m = 1815MHz, PCI = 98.

Fig. 5. Illustration of RSRP variation with Localization.

are highly possible to be similar to each other. In addition, experimental results conducted on the campus of Shanghai Jiao Tong University, as shown in Fig. 5, reveal a high correlation in signal RSRP observability for UEs located at adjacent positions. This suggests that the illumination patterns in the MBMC-R fingerprint arrays exhibit similarity for nearby positions.

According to these properties of the MBMC-R fingerprint, a SWKNN localization algorithm is proposed in this paper to improve the matching accuracy. This algorithm employs the sequential block-matching (SBM) method, as described in [50], which is suitable for matching continuous information and can improve matching accuracy. The cosine similarity distance [49] is utilized to quantify the similarity between two fingerprints. This is because the cosine similarity criteria are insensitive to zero values and, therefore, more suitable for sparse data, which is just the case with the MBMC-R fingerprint. The online fingerprint localization method primarily utilizes SBM and cosine similarity to calculate the similarity between the fingerprint to be located and the fingerprints in the offline database. Then, the WKNN algorithm is used to estimate the UE position. This algorithm is elaborated in Algorithm 1.

Therefore, the entire fingerprint localization process can be summarized into the following three steps.

Step 1: Obtain PCI and RSRP information for every LTE frequency. Grid the geographical area, and the number of grid points is N_{UE}. Obtain the position $\mathbf{p} = p_1, p_2, ..., p_{N_{\mathrm{UE}}}$ of the grid points. Sweep the area and obtain information about the LTE signals. Obtain PCI and RSRP information of every carrier band.

Step 2: Construct the offline database. Measure the RSRP and PCI corresponding to the different carrier bands of the UE at each received point, and save them in a matrix $F\mathrm{in}^{p_i}$. The fingerprints of all received points in the geographical area to be located from the offline fingerprint database $F\mathrm{in} = \{F\mathrm{in}^{p_1}, F\mathrm{in}^{p_2}, ..., F\mathrm{in}^{p_{N_{\mathrm{UE}}}}\}$.

Step 3: Online matching. By comparing the fingerprint $F\mathrm{in}^{p_i}$ of test point with the K_{SBM} consecutive fingerprints at geographical locations in an offline database, we can identify K nearest RPs whose features closely resemble the test point. It should be noted that the cosine similarity distance d_{ij} is

Algorithm 1: Online fingerprint localization algorithm

input : The offline MBMC-R fingerprint database $F\mathrm{in}$ calculated by (7). The geographic coordinates $\mathbf{p}$ of the reference points. The number of weights for WKNN K. The number of SBM matches K_{SBM}.

Offline mode

Calculate the SBM cosine similarity distance between the $F\mathrm{in}^{p_i}$ and the offline K_{SBM} $F\mathrm{in}^{p_j}$ fingerprints. The pseudocode is presented below:

for $j \in \{1, 2, ...N_{UE}\}$ **do**

  $F\mathrm{in}^{p_i}_{K_{\mathrm{SBM}}} = \mathrm{repeat}(F\mathrm{in}^{p_i}, K_{\mathrm{SBM}})$;

  $F\mathrm{in}^{p_j}_{K_{\mathrm{SBM}}} = [F\mathrm{in}^{p_{j-\frac{K_{\mathrm{SBM}}}{2}}}, ..., F\mathrm{in}^{p_j}, ..., F\mathrm{in}^{p_{j+\frac{K_{SBM}}{2}}}]$;

  $d_{ij} = \cos(\angle(F\mathrm{in}^{p_i}_{K_{\mathrm{SBM}}}, F\mathrm{in}^{p_j}_{K_{\mathrm{SBM}}}))$

end

Sort the distance calculated between the online fingerprint of user to be located and all offline fingerprint. Select K smallest distance values $d_{ij}^{k_{\mathrm{d}}}, k_{\mathrm{d}} = 1, ..., K$;

Calculate the weight w_i;

Select the first smallest K d_{ij} to calculate the $\hat{p}_i$;

output: $\hat{p}_i = (\hat{x}_i, \hat{y}_i)$: the estimated position.

adopted to quantify the dissimilarity between two fingerprints.

$$\begin{aligned} d_{ij} &= \cos(\angle(F\mathrm{in}^{p_i}_{K_{\mathrm{SBM}}}, F\mathrm{in}^{p_j}_{K_{\mathrm{SBM}}})) \\ &= \frac{F\mathrm{in}^{p_i}_{K_{\mathrm{SBM}}} \odot F\mathrm{in}^{p_j}_{K_{\mathrm{SBM}}}}{\left|F\mathrm{in}^{p_i}_{K_{\mathrm{SBM}}}\right| \cdot \left|F\mathrm{in}^{p_j}_{K_{\mathrm{SBM}}}\right|}, \end{aligned} \tag{9}$$

where $\odot$ is Hadamard product. We then calculate the weights and utilize the WKNN method to estimate the location $\hat{p}_i$ as follows

$$\mathrm{w}_i = \frac{d_{ij}^{k_{\mathrm{d}}}}{\sum_{k_{\mathrm{d}}=1}^{K} d_{ij}^{k_{\mathrm{d}}}}, \tag{10}$$

$$\hat{p}_i = \sum_{i=1}^{K} \mathrm{w}_i p_i. \tag{11}$$

C. Complexity Analysis and the Summary of Algorithm

Based on the above analysis, the fingerprint positioning method is determined. The computational complexity of the fingerprint method arises from the following components:

1) The complexity for step 1 is $O(\sum_{m=1}^{M_f} N_{\mathrm{m}})$. In order to acquire all RSRPs in the reference points, $\sum_{m=1}^{M_f} N_{\mathrm{m}}$ demodulations are required.

2) The complexity for step 2 is $O(N_{\mathrm{UE}})$. Thus, the complexity of offline database construction is $O(N_{\mathrm{UE}} \sum_{m=1}^{M_f} N_{\mathrm{m}})$.

3) The complexity for step 3 is $O(N_{\mathrm{UE}}^2 K_{\mathrm{SBM}} \sum_{m=1}^{M_f} N_{\mathrm{m}} + N_{\mathrm{UE}} \log K)$. The complexity for loop to calculate the cosine similarity distance is $O(N_{\mathrm{UE}}^2 K_{\mathrm{SBM}} \sum_{m=1}^{M_f} N_{\mathrm{m}})$. Besides, the

WKNN algorithm to calculate the estimation positioning is $O(N_{\mathrm{UE}} \log K)$.

Therefore, the complexity for the total fingerprint localization process is $O(N_{\mathrm{UE}}^2 K_{\mathrm{SBM}} \sum_{m=1}^{M_f} N_{\mathrm{m}} + N_{\mathrm{UE}} \log K)$. Compared with traditional RSRP fingerprints, the proposed MBMC-R fingerprint construction method increases the complexity of the algorithm by adding the distinction between the RSRPs corresponding to different carrier bands and PCIs. While SBM improves matching accuracy, it also increases the complexity of the algorithm.

V. CRLB of MBMC-R Fingerprint

In this section, we derive the CRLB bound of the SWKNN algorithm with the MBMC-R fingerprint. We further analyze the impacts of the number of instantaneously observed signal carrier bands on the CRLB and demonstrate the superiority of utilizing multiband and multicell RSRP information.

A. The Derivation of CRLB

The MBMC-R fingerprint includes multiband and multicell RSRP information, which is transmitted from multiple BSs. Assume that the RSRP collected from different BSs follows a multivariate normal distribution, which aligns with the assumption of RSRP following a normal distribution. Therefore, each vector of RSRP measurements from a BS is assumed to exhibit independent and identical distribution characteristics, and the joint probability density function obtained from different BSs can be defined as

$$f_{p_i}\left(P_1, ...P_{M_f}\right) = \prod_{m=1}^{M_f} \left(\prod_{k_m=1}^{N_m} \frac{1}{\sqrt{2\pi}\sigma_m} \exp\left(-\frac{{\xi_m}^2}{2{\sigma_m}^2}\right)\right), \tag{12}$$

where $\xi_m = P_{ik_m} - P_{0k_m} - L(f_c^m) - \beta_{k_m} \log d_{ik_m}$ is mentioned in Section II B. σ_m^2 denotes the variance corresponding to the mth carrier band. N_m represents the number of PCIs associated with the mth carrier band.

Let $\hat{p}_i = (\hat{x}_i, \hat{y}_i)$ be the unbiased estimate of the ith real location $p_i = (x_i, y_i)$ and the position of the k_mth BS is denoted as $p_{k_m} = (x_{k_m}, y_{k_m})$. If $\hat{p}_i$ is determined based on the unbiased estimate of the measurement (e.g., RSRP) P_{ik_m} at the ith real location, the FIM [42] is utilized to derive the following relationships, which provide the lower bound of the variance of $\hat{p}_i$ as follows

$$E\left\{\left(\hat{p}_i - p_i\right)\left(\hat{p}_i - p_i\right)^T\right\} \geq J(p_i)^{-1}, \tag{13}$$

where $E\{\bullet\}$ denotes the expectation operation and $(\bullet)^{-1}$ denotes the inverse of a matrix. $J(p_i)$ represents the FIM with respect to p_i as

$$\begin{aligned} J(p_i) &= E\left\{\frac{\partial^2 \ln f_{p_i}\left(P_1, ...P_{M_f}\right)}{\partial p_i^2}\right\} \\ &= \begin{bmatrix} J_{x_i x_i}(\xi_m) & J_{x_i y_i}(\xi_m) \\ J_{y_i x_i}(\xi_m) & J_{y_i y_i}(\xi_m) \end{bmatrix}. \end{aligned} \tag{14}$$

Therefore, the FIM can be expressed as

$$V_{M_f} = \frac{\lambda_{iM_f}}{\ln 10 \eta_{iM_f}}, \tag{15}$$

where

$$x_{ik_m} = \frac{\beta_{k_m}}{\sigma_m} \frac{(x_i - x_{k_m})}{{d_{ik_m}}^2}, \tag{16}$$

$$y_{ik_m} = \frac{\beta_{k_m}}{\sigma_m} \frac{(y_i - y_{k_m})}{{d_{ik_m}}^2}, \tag{17}$$

$$\lambda_{iM_f} = \sum_{m=1}^{M_f} \sum_{k_m=1}^{N_m} \left({x_{ik_m}}^2 + {y_{ik_m}}^2\right), \tag{18}$$

$$\eta_{iM_f} = \sum_{m=1}^{M_f} \sum_{k_m=1}^{N_m} {x_{ik_m}}^2 \sum_{m=1}^{M_f} \sum_{k_m=1}^{N_m} {y_{ik_m}}^2 - \left(\sum_{m=1}^{M_f} \sum_{k_m=1}^{N_m} x_{ik_m} y_{ik_m}\right)^2. \tag{19}$$

The detailed derivations are given in Appendix A.

B. Impact Factors for CRLB

Theorem 1. *The introduction of additional carrier bands leads to a decrease in the CRLB, except for the case when* $p_{M_f+1} = p_{k_m}, k_m = 1, ..., M_f$.

Proof. The detailed derivations for Theorem 1 are given in Appendix B. □

Theorem 2. *The increasing number of cells leads to a decrease in the CRLB, except for the case when* $p_{N_m+1} = p_{k_m}, k_m = 1, ..., N_m$.

Proof. The proof is omitted due to space limitations. The derivation method is similar to that used by Theorem 1. □

Theorem 1 and Theorem 2 explains that the variance of positioning error is influenced by the number of carrier bands and cells. An increase in the number of carrier bands or cells can reduce the positioning error. However, when the number of carrier bands or cells is extremely large, the computational complexity of the fingerprint localization algorithm becomes intolerable. Furthermore, equation (15) shows that the location error of the proposed fingerprint depends on σ_m for different center frequencies of LTE signals. The positioning error grows as the shadow fading factor increases. Besides, the distance between the UE and BS also affects the variance of the localization error. When the distance between the UE and BS diminishes, the variance of positioning error increases.

VI. Measurement Results

In this section, we introduce the data collection method and experimental results. A set of experiments has been conducted in order to evaluate the effectiveness of the proposed architectures to clarify the superiority of the proposed algorithm compared with the traditional fingerprint localization algorithm.

A. Data Collection

The real time measurement data are collected along the tree-lined roads on the campus of Shanghai Jiao Tong University from September 10, 2023 to September 24, 2023. The outdoor trajectories, including Street 1 and Street 2, are depicted in Fig. 6. For Street 1, a Huawei Mate20 mobile phone is utilized to collect LTE signals across 13 carrier bands. The total length of the road is approximately 1326.620 m, with an average sampling interval of 6.378 m. In the case of Street 2, the USRP device is used to collect LTE signals at 9 carrier bands. The total length of the road is approximately 1700.302 m, and the sampling interval is 5.844 m. We have used 13 carrier bands and 66 PCI numbers for LTE signals in Street 1, and 9 carrier bands and 60 PCI numbers for LTE signals in Street 2. At a single position, the UE can receive signals from at least nine carrier bands in the LTE network.

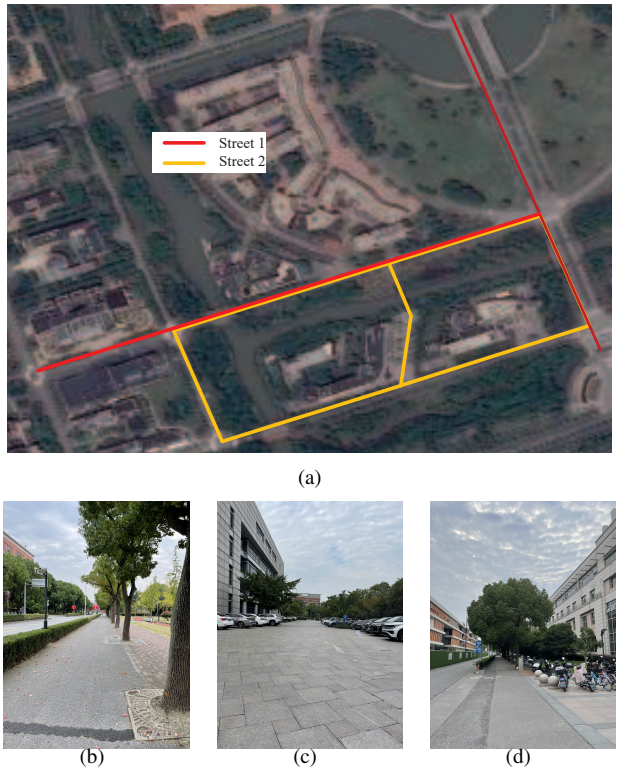

Fig. 6. The satellite and photographs of the localization area in Shanghai Jiao Tong University. (a) Satellite map. Different trajectories of the outdoor sequences are visualized with different colors in the map. (b-d) Real scene.

The data can be acquired by mobile phone or USRP. Mobile phones can directly obtain RSRP, PCI, carrier band, and coordinate information. Next, we focus on the process of using USRP for signal acquisition. The multiband and multicell LTE data are acquired by the setup illustrated in Fig. 7 to collect data from different BSs. To collect the LTE I/Q signals, we run Gnuradio on an ACP-2010 Industrial Personal Computer (IPC) with a USRP B210 platform. The computer runs on the Ubuntu 16.04 operating system. The configuration of the ACP-2010 IPC includes 32 GB of DDR4 RAM, a 1TB HDD, and USB 3.0 interfaces. The IPC, connected to the USRP through USB 3.0 interfaces, serves as a system controller and data recording unit. The longitude and latitude coordinate information is obtained by the NovAtel FANS System with a Lenovo T440P processor. Subsequently, the MATLAB LTE toolbox is utilized to obtain the carrier band, PCI, and RSRP information. Finally, we construct the proposed MBMC-R fingerprint using the method proposed in Section III.

Remark 2. *It is worth noting that this experiment utilizes GNSS to collect location tags to verify fingerprint accuracy. Other precise positioning methods, such as sensor-based positioning, can also be employed to obtain location tags and replace GNSS. Regarding the acquisition of offline tags, the proposed algorithm offers a high degree of freedom and flexibility in tag selection, making the proposed algorithm versatile and scalable.*

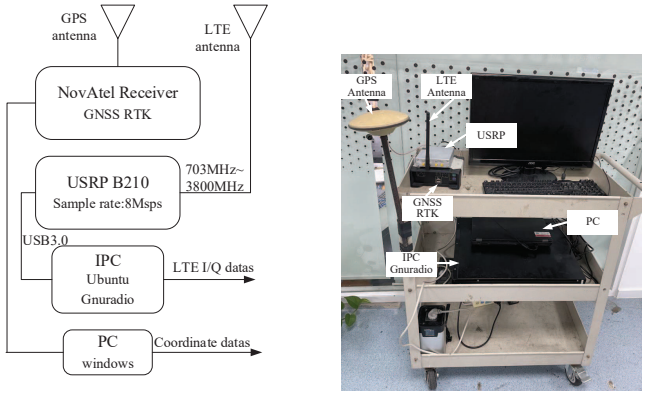

(a) Block scheme (b) Experimental setup

Fig. 7. Measurement system.

B. Performance Results

In this section, the performance of the MBMC-R fingerprint localization algorithm is evaluated in multiple urban wireless propagation scenarios. The experiments adopt two devices, e.g., mobile phone and USRP, to collect LTE signals and construct fingerprints. The leave-one-out cross-validation method [51] is adopted in the localization accuracy evaluation. Furthermore, the performance is evaluated from multiple perspectives, including localization accuracy, the impact of system parameters, time overhead, etc.

Fig. 8 illustrates the variation of the CRLB with an increasing number of carrier bands and the change in CRLB with the average distance between the BSs and the UEs. It can be observed that the CRLB decreases as the number of carrier bands increases. Moreover, when the number of carrier bands is sufficiently large, the change in CRLB becomes more gradual. On the other hand, the CRLB increases as the average distance between BSs and UEs increases. These results align with the theoretical analysis, confirming the accuracy of the theoretical derivation.

Fig. 9 displays the cumulative distribution function (CDF) of localization inaccuracies with MBMC-R, CSI [48], radio channel [25] and RSSI [28] fingerprints by SWKNN approach. Since mobile phones are unable to obtain CSI directly, LTE signals obtained by USRP are chosen for the experiment.

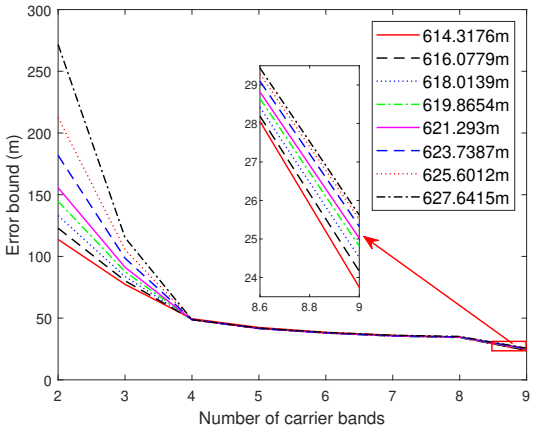

Fig. 8. Comparison under different numbers of carrier bands and the average distance for BSs and UE.

Taking the 67% point of the CDF as the localization accuracy criteria, MBMC-R, RSSI, CSI, radio channel fingerprint localization method achieve the accuracy of 21.947 m, 108.724 m, 181.105 m, and 215.681 m, respectively. Taking the 90% point of the CDF as the localization accuracy criterion, MBMC-R, RSSI, CSI, and radio channel fingerprint localization methods achieve the accuracies of 47.217 m, 191.614 m, 302.710 m, and 360.665 m, respectively. The CSI and radio channel fingerprint methods provide the lowest accuracy for that the multiple-path information is deeply coupled in CSI and CSI fingerprint only uses one carrier band. The MBMC-R and RSSI, fingerprint localization algorithms, provide improved location accuracy due to their ability to capture various features such as RSRP/RSSI, PCI, and frequency information. Besides, RSRP/RSSI, which is the average received signal power, reduces the impact of environment noise. Incorporating these diverse features captures a richer set of information about the environment, making it more resilient to variations and enhancing localization accuracy. Furthermore, the proposed MBMC-R method achieves more accurate positioning than the RSSI algorithm due to the higher information dimensions and more PCI information in the fingerprint.

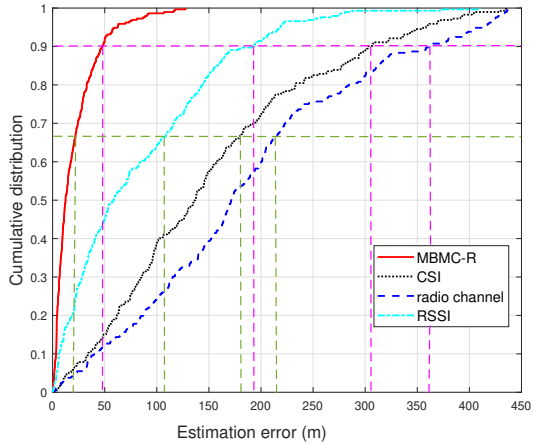

Fig. 9. Comparison of CDFs among different algorithms with USRP collected data.

Table I presents the positioning errors for the compared algorithms, respectively, the WKNN localization method with cosine similarity distance (referred to WKNN+cos), the WKNN localization method with Euclid distance (referred to WKN+Euclid), the SWKNN localization method with cosine similarity distance (referred to SWKNN+cos), and the SWKNN localization method with Euclid distance (referred to SWKNN+Euclid) by using the MBMC-R fingerprint. It is evident that SWKNN+cos achieves the smallest error among the methods compared. SBM considers the spatial relationship between consecutive positions and leverages the contextual information to refine the localization estimate. This contextual awareness significantly enhances positioning accuracy compared to the WKNN algorithm, which treats positions independently. The cosine similarity criterion provides better performance for fingerprint matching than Euclidean distance due to its robustness to scale, improved discrimination, and higher efficiency.

Fig. 10 shows the estimation results of the MBMC-R SWKNN method on street 2. The figure shows the actual test points from the offline database, the estimated points, and the deviations between the real and estimated results. The estimated results are predominantly in the offline fingerprint collection route. However, due to the similarities in the data collection environment, certain data points may deviate from their actual positions, introducing ambiguity into the results.

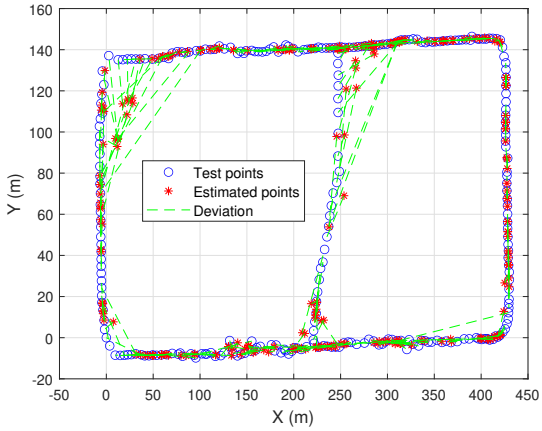

Fig. 10. Localization estimation results of the proposed method on street 2.

The CRLB analysis results illustrate that position accuracy primarily depends on the number of carrier bands. Large values of M_f result in higher positioning accuracy. Therefore, in Fig. 11, the number of carrier bands is increased from 1 to 9 in an outdoor scene to evaluate the positioning accuracy by utilizing our proposed localization approach. Taking the 67 % point of CDF as a reference point, the figure indicates that the MBMC-R SWKNN method with $M_f = 1 - 9$ achieves localization accuracies of 101.884 m, 77.100 m, 61.693 m, 45.490 m, 44.845 m, 32.066 m, 28.283 m, 25.402 m, and 21.947m accuracy. The experimental results align with the derived results from the CRLB, indicating consistency between them. Additionally, as the number of carrier bands increases, the change in positioning accuracy becomes more gradual and less pronounced.

TABLE I
THE POSITION ERROR OF FOUR POSITION METHODS, UNIT: M.

equipment	Item	WKNN+cos	WKNN+Euclid	SWKNN+cos	SWKNN+Euclid
USRP	50% error	17.452	18.491	12.387	18.240
	67% error	26.314	31.037	21.947	29.911
	75% error	33.403	36.914	28.364	37.383
	95% error	60.209	98.183	62.418	137.578
	Average error	23.237	29.405	20.413	33.041
phone	50% error	7.963	10.356	6.921	6.757
	67% error	13.023	15.636	11.607	11.655
	75% error	17.561	21.183	15.541	15.616
	95% error	46.620	53.381	44.968	48.218
	Average error	13.786	16.625	13.340	15.207

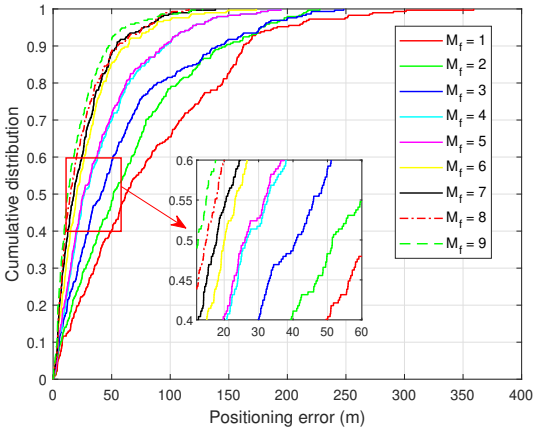

Fig. 11. Localization estimation results of the proposed method with different numbers of carrier bands on Street 2.

Fig. 12 shows the estimation results of the MBMC-R SWKNN method in street 1. The figure shows the actual test points, the estimated points, and the deviations between them. The estimated results are mostly in the offline fingerprint collection route. Compared to the results of Street 2, the localization results of Street 1 exhibit smaller deviations between the true and estimated positions. This can be attributed to the relatively simpler collection route of Street 1, while also incorporating a greater number of carrier bands to construct the fingerprint.

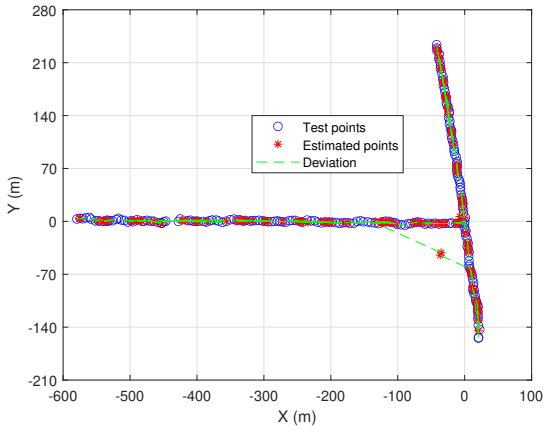

Fig. 12. Localization estimation results of the proposed method on street 1.

Fig. 13 illustrates the localization accuracy as the number of carrier bands increases from 1 to 13 in the outdoor scene of Street 1. Taking the 67 % point of CDF as a reference point, the figure demonstrates that the MBMC-R SWKNN method with $M_f = 1 - 13$ realizes location with 277.684m, 95.332m, 26.530m, 25.277m, 23.488m, 20.657m, 20.304m, 11.607m, 11.607m, 11.607m m, 11.607m m, 11.607m, and 11.607m accuracy. The experimental results align with the derived results from the CRLB. Furthermore, it is observed that as the number of carrier bands increases, the variations in positioning accuracy become more gradual or less significant, which is consistent with the simulation results for the CRLB.

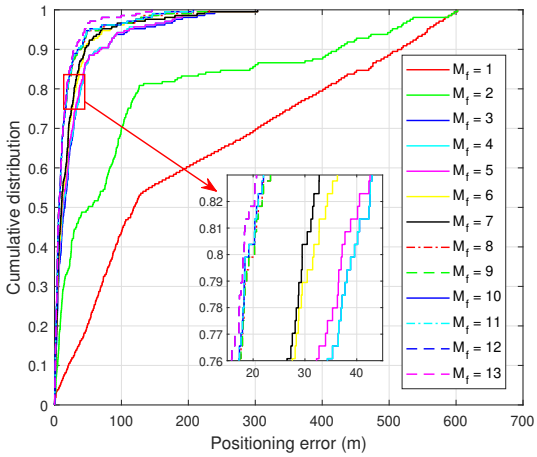

Fig. 13. Localization estimation results of the proposed method with different numbers of carrier bands on Street 1.

The positioning performance depends not only on positioning accuracy but also on position time overhead. For the above methods, the fingerprints and the corresponding coordinates are calculated and saved by MATLAB R2022b. Our experiment is carried out on a workstation equipped with Intel(R) Core(TM) i5-10400F CPU and 16 GB of RAM. During the experiment, the unknown position of 292 points is estimated, and the average positioning time for each unknown point is calculated. The time overhead of different position approaches is shown in Table II. As we can see, the proposed MBMC-R fingerprint localization method is able to provide a location estimation in less than 1s, outperforming the other methods. The MBMC-R fingerprint localization method enhances positioning accuracy and reduces computational time

TABLE II
THE POSITION TIME OVERHEAD OF FOUR FINGERPRINT POSITION METHODS, UNIT: S.

Method	MBMC-R	CSI	radio channel	RSSI
Time	0.0147	8.451	0.0350	0.0146

TABLE III
LOCALIZATION RESULTS BASED ON USRP DATASET (292 DATA) AND PROPOSED MBMC-R FINGERPRINT.

Fingerprint	MBMC-R			
Methods	SWKNN	MLP	CNN	DCNN
Average error (m)	20.413	111.997	204.17	141.780
Time (s)	0.0147	0.200	0.0264	0.0256

compared to other CSI-based fingerprint localization methods.

Table III compares the proposed SWKNN algorithm with multilayer perceptron (MLP), CNN [36], and deep convolutional neural network (DCNN) [37] algorithms in USRP dataset. The MLP has 1024 neurons in hidden layers 1, 2, and 3, and 2 neurons in the output layer. Both CNN and DCNN adopt regression models. It is worth noting that all these positioning techniques employ the MBMC-R fingerprint. Table III shows that the SWKNN algorithm has the shortest localization time and the best accuracy compared to MLP, CNN, and DCNN methods. The SWKNN method utilizes data from the training dataset for matching. It adjusts the matching results with weights to effectively reduce the influence of noise and outliers, making localization more accurate and robust. In addition, traversing and matching the small-size training dataset requires little time, enabling quick positioning. The MBMC-R fingerprint achieves richer and higher-dimensional fingerprint characteristics strongly correlated with geographical locations. Due to the high similarity between fingerprints of adjacent positions, the SWKNN algorithm can provide higher positioning accuracy than neural network matching algorithms.

By utilizing the CSI fingerprint, the localization results of SWKNN, MLP, CNN [36], and DCNN [37] are shown in Table IV. The CSI fingerprint only uses one carrier band and cell, as shown in (2). In the small-size USRP dataset, the localization accuracy of CSI is relatively low. Compared to the CSI fingerprints, by utilizing the MBMC-R fingerprint, the SWKNN algorithm improves the localization accuracy by over 80%. The proposed MBMC-R fingerprint outperforms the CSI fingerprint because the impact of noise is reduced, and space and frequency diversity are utilized.

Increasing the value of K_{SBM} raises the computational cost, consequently increasing the time complexity of the localization algorithm. This occurs because more computational resources are required to compare the UE signal with multiple candidate signals to determine the best match at each matching step. To select the optimal number of sequential matching steps, we consider the balance between the computation cost and accuracy. As shown in Tab. V, the SWKNN method with $K_{\text{SBM}} = 3$ increases the computational cost while significantly reducing positioning accuracy. Therefore, the SWKNN method chooses $K = 3$ and $K_{\text{SBM}} = 3$ as the optimal sequential matching value.

Fig. 14 depicts the average localization error of the proposed MBMC-R SWKNN algorithm with different values of K_{SBM} and K. As shown in Fig. 14, the minimal average positioning error occurs when $K = 3, K_{\text{SBM}} = 3$. With a small value of K and K_{SBM}, the algorithm tends to be more sensitive to outliers or noisy data points. On the other hand, with a large value of K and K_{SBM}, the algorithm may lose its ability to capture local patterns effectively. By choosing $K = 3$ and $K_{\text{SBM}} = 3$, a balance is struck between these extremes, resulting in a smoothing effect. It considers the contributions of the three nearest neighbors without being overly influenced by individual outliers, thus providing a more stable and reliable prediction.

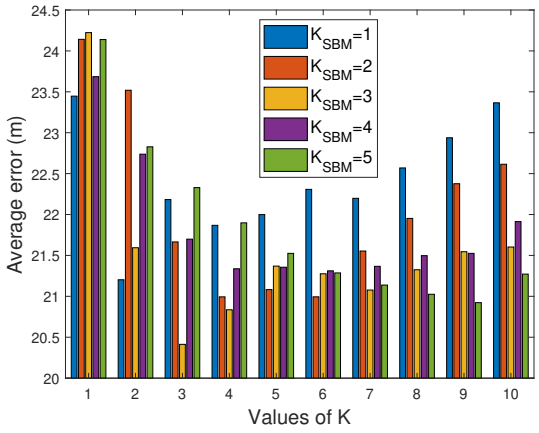

Fig. 14. The average positioning error of SWKNN algorithm with different K and K_{SBM}.

TABLE IV
LOCALIZATION RESULTS BASED ON USRP DATASET (292 DATA) AND CSI FINGERPRINT.

Fingerprint	CSI			
Methods	SWKNN	MLP	CNN	DCNN
Average error (m)	152.265	225.219	234.193	181.987
RMSE	183.236	257.188	258.002	205.975

TABLE V
THE POSITION TIME OVERHEAD OF DIFFERENT K_{SBM} FOR PROPOSED FINGERPRINT LOCALIZATION METHOD, UNIT: S.

Number of SBM	1	2	3	4	5
Time	0.0967	0.0122	0.0147	0.0169	0.0199

C. Performance Results with Public database

The proposed method's superiority is verified using the Deep MIMO dataset [52], which includes more carrier bands, cells, and signal types. The proposed algorithm is not limited to LTE signals but applies to all cellular signals. This dataset is acquired from the widely used ray-tracing simulator Remcom Wireless InSite and validated with real-world channel measurements. The parameters are summarized in TableVI. For LTE signals, the center frequency is 3.4 GHz with a 20 MHz bandwidth. For 5G signals, the center frequencies are 3.5 GHz, 28 GHz, and 60 GHz, with bandwidths of 100 MHz, 200 MHz, and 2 GHz, respectively.

The dataset consists of outdoor urban street scenarios with dimensions of 550 m $\times$ 36 m. The reference fingerprint

TABLE VI
MAJOR WIRELESS PARAMETERS FOR DEEP MIMO DATASET.

Parameters	Value
Normalized antenna spacing	0.5
Number of paths	25
BS antenna	ULA
Subcarrier number	64
Number of active BS in each carrier band	12
Grid spacing	1 m
Height of BS	6 m
Height of users	2 m
Number of users to localization	5000
Signal type	LTE, 5G

database consists of 551 y-axis and 37 x-axis positions, collected from a grid of 20387 locations. The test database contains 5000 randomly distributed test points.

TABLE VII
LOCALIZATION RESULTS BASED ON DEEP MIMO DATASET (20387 DATA) AND PROPOSED MBMC-R FINGERPRINT.

Fingerprint	MBMC-R			
Methods	SWKNN	MLP	CNN	DCNN
Average error (m)	0.847	177.720	19.996	8.517
Online time (s)	0.0446	0.00210	0.00461	0.00458

Table VII compares the proposed SWKNN algorithm with MLP, CNN [36], and DCNN [37] algorithms in Deep MIMO dataset. Table VII depicts the SWKNN achieves higher accuracy compared to other localization methods. The SWKNN algorithm improves the localization accuracy by 90% compared to neural network matching methods. The reason is that the SWKNN method can adaptively select features for localization and is robust to environment changes. Furthermore, the superior localization accuracy of the proposed SWKNN algorithm over the CNN algorithm is attributed to the fact that the SWKNN algorithm is suitable for MBMC-R fingerprints. Although the SWKNN takes longer to test online than neural networks, its offline training time is much shorter. In contrast, neural networks must design and adjust network parameters for different training datasets, requiring abundant computing resources and a large amount of offline training time, which limits practical applications to a certain extent.

TABLE VIII
LOCALIZATION RESULTS BASED ON DEEP MIMO DATASET (20387 DATA) AND CSI FINGERPRINT.

Fingerprint	CSI			
Methods	SWKNN	MLP	CNN	DCNN
Average error (m)	172.830	150.72	186.060	177.857
RMSE	206.46	175.81	224.695	211.761

The positioning results of different localization methods for CSI fingerprint are shown in Table VIII. In the large-size DeepMIMO dataset, the accuracy of the CSI fingerprint is also low, as shown in Table VIII. Compared to the CSI fingerprints, by utilizing the MBMC-R fingerprint, the SWKNN algorithm improved the localization accuracy by over 99% for the proposed MBMC-R fingerprint.

The proposed MBMC-R SWKNN algorithm achieves the highest localization accuracy in both USRP and Deep MIMO datasets. On the one hand, the proposed MBMC-R fingerprint outperforms the CSI fingerprint because the MBMC-R fingerprint reduces the impact of noise and utilizes space and frequency diversity. On the other hand, compared to neural network matching methods, the SWKNN algorithm improves the localization accuracy by 90%. The SWKNN algorithm fully leverages the continuous features of the MBMC-R fingerprints in spatial and frequency dimensions. Multiple-path information is deeply coupled in CSI, and suitable neural networks need to be designed to learn the relationship between CSI and geographic information. In conclusion, by jointly improving fingerprint features and matching algorithms, our algorithm has achieved the best localization performance.

VII. CONCLUSIONS

In this study, a new type of multiband multicell RSRP fingerprint, named MBMC-R, is proposed. The MBMC-R fingerprint shows a clearer and closer relationship with the actual position, improving the positioning accuracy. A localization algorithm, SWKNN, is used to perform position estimation by utilizing MBMC-R fingerprints. The CRLB has been derived to explain the positioning accuracy of MBMC-R fingerprints and simultaneously confirm that multiband and multicell fingerprints can significantly enhance the localization accuracy of the algorithm. Experimental results conducted on the campus of Shanghai Jiao Tong University validate the superior performance of the proposed method compared to the current algorithms mentioned in the references. Our method is not only applicable to LTE signals but also suitable for cellular signals such as 5G. In addition, we will collect sensor-based tags and validate the performance of the proposed algorithm for localization in environments where GNSS is entirely unavailable in future work. Further, combining 5G PRS with the proposed algorithm and using their respective advantages to improve positioning accuracy is precious research and a challenge. We will work on this in future work.

APPENDIX A

FIM can be solved by (14), and the first order derivative $E\left\{\frac{\partial \ln f_{p_i}(P_1,...P_{M_f})}{\partial x_i}\right\}$ is solved as

$$-E\left\{\frac{\partial}{\partial x_i}\sum_{m=1}^{M_f}\sum_{k_m=1}^{N_m}\left(\ln\frac{1}{\sqrt{2\pi}\sigma_m}-\frac{{\xi_m}^2}{2{\sigma_m}^2}\right)\right\}$$

$$=-E\left\{\frac{\partial}{\partial d_{ik_m}}\sum_{m=1}^{M_f}\sum_{k_m=1}^{N_m}\left(\ln\frac{1}{\sqrt{2\pi}\sigma_m}-\frac{{\xi_m}^2}{2{\sigma_m}^2}\right)\frac{\partial d_{ik_m}}{\partial x_i}\right\}$$

$$=-E\left\{\sum_{m=1}^{M_f}\sum_{k_m=1}^{N_m}\left(\frac{\xi_m}{{\sigma_m}^2\ln 10}\beta_{k_m}\frac{1}{d_{ik_m}}\frac{\partial d_{ik_m}}{\partial x_i}\right)\right\}. \quad (20)$$

Then, the second order derivative of $E\left\{\frac{\partial^2 \ln f_{p_i}(P_1,...P_{M_f})}{\partial x_i^2}\right\}$ is solved as

$$J_{x_ix_i}(P_1,...P_{M_f})=\sum_{m=1}^{M_f}\sum_{k_m=1}^{N_m}\left(\frac{1}{{\sigma_m}^2\ln 10^2}{\beta_{k_m}}^2\frac{1}{{d_{ik_m}}^2}\frac{\partial d_{ik_m}}{\partial x_i}\right), \quad (21)$$

where

$$\frac{\partial d_{ik_m}}{\partial x_i} = \frac{(x_i - x_{k_m})}{d_{ik_m}}. \tag{22}$$

Substituting (22) into (21), (21) can be derived as

$$J_{x_i x_i}(P_1, ...P_{M_f}) = \sum_{m=1}^{M_f} \sum_{k_m=1}^{N_m} \left(\frac{{\beta_{k_m}}^2}{{\sigma_m}^2 \ln 10^2} \frac{(x_i - x_{k_m})^2}{{d_{ik_m}}^4} \right). \tag{23}$$

Similarly, we can derive that

$$J_{y_i y_i}(P_1, ...P_{M_f}) = \sum_{m=1}^{M_f} \sum_{k_m=1}^{N_m} \left(\frac{{\beta_{k_m}}^2}{{\sigma_m}^2 \ln 10^2} \frac{(y_i - y_{k_m})^2}{{d_{ik_m}}^4} \right), \tag{24}$$

$$\begin{aligned} &J_{x_i y_i}(P_1, ...P_{M_f}) \\ &= \sum_{m=1}^{M_f} \sum_{k_m=1}^{N_m} \left(\frac{{\beta_{k_m}}^2}{{\sigma_m}^2 \ln 10^2} \frac{(x_i - x_{k_m})(y_i - y_{k_m})}{{d_{ik_m}}^4} \right). \end{aligned} \tag{25}$$

This concludes the derivation process of (15).

APPENDIX B

When an additional $(M_f + 1)$th carrier bands LTE signal is added to the MBMC-R fingerprint, the CRLB can be represented as

$$V_{M_f+1} = \frac{\lambda_{iM+1}}{\ln 10 \eta_{iM+1}}, \tag{26}$$

where

$$\lambda_{iM_f+1} = \lambda_{iM_f} + \sum_{k_{M_f+1}=1}^{N_{M_f+1}} \left({x_{ik_{M_f+1}}}^2 + {y_{ik_{M_f+1}}}^2 \right), \tag{27}$$

$$\begin{aligned} \eta_{iM_f+1} &= \eta_{iM_f} + \sum_{m=1}^{M_f} \sum_{k_m=1}^{N_m} x_{ik_m}^2 \sum_{k_{M_f+1}=1}^{N_{M_f+1}} y_{ik_{M_f+1}}^2 \\ &+ \sum_{m=1}^{M_f} \sum_{k_m=1}^{N_m} y_{ik_m}^2 \sum_{k_{M_f+1}=1}^{N_{M_f+1}} x_{ik_{M_f+1}}^2 + \sum_{k_{M_f+1}=1}^{N_{M_f+1}} x_{ik_{M_f+1}}^2 \sum_{k_{M_f+1}=1}^{N_{M_f+1}} y_{ik_{M_f+1}}^2 \\ &- 2 \left(\sum_{m=1}^{M_f} \sum_{k_m=1}^{N_m} x_{ik_m} y_{ik_m} \right) \left(\sum_{k_{M_f+1}=1}^{N_{M_f+1}} x_{ik_{M_f+1}} y_{ik_{M_f+1}} \right) \\ &- \left(\sum_{k_{M_f+1}=1}^{N_{M_f+1}} x_{ik_{M_f+1}} y_{ik_{M_f+1}} \right)^2. \end{aligned} \tag{28}$$

To prove that an increased number of carrier bands enhances fingerprint localization accuracy, it is sufficient to demonstrate the following formula

$$V_{M_f} - V_{M_f+1} = \frac{\lambda_{iM_f} \eta_{iM_f+1} - \lambda_{iM_f+1} \eta_{iM_f}}{\ln 10 \eta_{iM_f} \eta_{iM_f+1}} \geq 0. \tag{29}$$

The denominator of (29) is non-negative since $\eta_{iM_f}, \eta_{iM_f+1} \geq 0$ and $\ln 10 > 0$. It can be proven through mathematical induction that $\eta_{iM_f}, \eta_{iM_f+1} \geq 0$, and the induction proof of this inequality is omitted for conciseness.

Next, we analyze the non-negativity of the numerator in (29). There holds

$$\begin{aligned} &\lambda_{iM_f} \eta_{iM_f+1} - \lambda_{iM_f+1} \eta_{iM_f} \\ &\geq \left(\begin{array}{l} \sqrt{\lambda_{iM_f} \sum_{m=1}^{M_f} \sum_{k_m=1}^{N_m} {x_{ik_m}}^2 - \eta_{iM_f}} \sum_{k_{M_f+1}=1}^{N_{M_f+1}} y_{ik_{M+1}} \\ -\sqrt{\lambda_{iM_f} \sum_{m=1}^{M_f} \sum_{k_m=1}^{N_m} {y_{ik_m}}^2 - \eta_{iM_f}} \sum_{k_{M+1}=1}^{N_{M_f+1}} x_{ik_{M_f+1}} \end{array} \right)^2 \\ &+ 2 \sqrt{\lambda_{iM_f} \sum_{m=1}^{M_f} \sum_{k_m=1}^{N_m} {x_{ik_m}}^2 - \eta_{iM_f}} \sum_{k_{M_f+1}=1}^{N_{M_f+1}} y_{ik_{M_f+1}} \\ &\times \sqrt{\lambda_{iM_f} \sum_{m=1}^{M_f} \sum_{k_m=1}^{N_m} {y_{ik_m}}^2 - \eta_{M_f}} \sum_{k_{M_f+1}=1}^{N_{M_f+1}} x_{ik_{M_f+1}} \\ &-2\lambda_{iM_f} \left(\sum_{m=1}^{M_f} \sum_{k_m=1}^{N_m} x_{ik_m} y_{ik_m} \right) \left(\sum_{k_{M_f+1}=1}^{N_{M_f+1}} x_{ik_{M_f+1}} y_{ik_{M_f+1}} \right) \\ &\geq \left(\begin{array}{l} \sqrt{\lambda_{iM_f} \sum_{m=1}^{M_f} \sum_{k_m=1}^{N_m} {x_{ik_m}}^2 - \eta_{iM_f}} \sum_{k_{M_f+1}=1}^{N_{M_f+1}} y_{ik_{M_f+1}} \\ -\sqrt{\lambda_{iM_f} \sum_{m=1}^{M_f} \sum_{k_m=1}^{N_m} {y_{ik_m}}^2 - \eta_{iM_f}} \sum_{k_{M_f+1}=1}^{N_{M_f+1}} x_{ik_{M_f+1}} \end{array} \right)^2 \\ &\geq 0. \end{aligned} \tag{30}$$

The case $V_{M_f} - V_{M_f+1} = 0$ arises only for the scenario $p_{k_{M_f+1}} = p_{k_m}$. In the real environment, the locations of the BSs with different carrier bands must be distinct. Thus, there holds $V_{M_f} - V_{M_f+1} > 0$, and adding a BS with different carrier bands does indeed lower the CRLB of the localization method.

This concludes the proof process for Theorem 1.

REFERENCES

[1] S. Zekavat, R. M. Buehrer, G. D. Durgin, et al., "An overview on position location: Past, present, future." *Int. J. Wireless Inf. Networks*, vol. 28, no. 1, pp. 45-76, Mar. 2021.

[2] F. Zafari, A. Gkelias and K. K. Leung, "A survey of indoor localization systems and technologies," *IEEE Commun. Surv. Tutorials*, vol. 21, no. 3, pp. 2568-2599, Apr. 2019.

[3] N. Saeed, H. Nam, T. Y. Al-Naffouri, et al., "A state-of-the-art survey on multidimensional scaling-based localization techniques," *IEEE Commun. Surv. Tutorials*, vol. 21, no. 4, pp. 3565-3583, Jun. 2019.

[4] P. Wang, Y. Wang and Y. J. Morton, "Signal tracking algorithm with adaptive multipath mitigation and experimental results for LTE positioning receivers in urban environments," *IEEE Trans. Aerosp. Electron. Syst.*, vol. 58, no. 4, pp. 2779-2795, Aug. 2022.

[5] A. Kirmaz, T. Sahin, D. S. Michalopoulos, et al., "ToA and TDoA estimation using artificial neural networks for high-accuracy ranging," *IEEE J. Sel. Areas Commun.*, vol. 41, no. 12, pp. 3816-3830, Dec. 2023.

[6] K. Radnosrati, C. Fritsche, F. Gunnarsson, et al., "Localization in 3GPP LTE based on one RTT and one TDOA observation," *IEEE Trans. Veh. Technol.*, vol. 69, no. 3, pp. 3399-3411, Mar. 2020.

[7] W. Luo, Z. Ni and Y. Ren, "A novel dual-band base station antenna with parasitic structure," in *2020 IEEE MTT-S Int. Conf. NEMO.*, 2020, pp. 1-3.

[8] S. J. Maeng, O. Ozdemir, M. L. Sichitiu, et al., "AERIQ: SDR-based LTE I/Q measurement and analysis framework for air-to-ground propagation modeling," in *2023 IEEE Aerosp. Conf.*, 2023, pp. 1-11.

[9] M. Jamalabdollahi, S. Zekavat and K. Pahlavan, "High-resolution OFDM-based sensor node ranging within in-homogeneous media of human body," *IEEE Trans. Wireless Commun.*, vol. 18, no. 4, pp. 2286-2298, Apr. 2019.

[10] P. C. Ng, P. Spachos, J. She, et al., "A kernel method to nonlinear location estimation with RSS-based fingerprint," *IEEE Trans. Mob. Comput.*, vol. 22, no. 8, pp. 4388-4404, Aug. 2023.

[11] A. M. Hossain, H. N. Van, Y. Jin, et al., "Indoor localization using multiple wireless technologies," in *Proc. IEEE Int. Conf. Mobile Adhoc Sens. Syst.*, 2007, pp. 1-8.

[12] M. B. Kjærgaard and C. V. Munk, "Hyperbolic location fingerprinting: A calibration-free solution for handling differences in signal strength (concise contribution)," in *2008 Sixth Annual IEEE Int. Conf. Pervasive Comput. Commun. (PerCom)*, 2008, pp. 110-116.

[13] X. Zhu, T. Qiu, W. Qu, et al., "BLS-location: A wireless fingerprint localization algorithm based on broad learning," *IEEE Trans. Mob. Comput.*, vol. 22, no. 1, pp. 115-128, Jan. 2023.

[14] P. Li, X. Yang, Y. Yin, et al., "Smartphone-based indoor localization with integrated fingerprint signal," *IEEE Access*, vol. 8, pp. 33178-33187, Feb. 2020.

[15] J. Fontaine, B. Van Herbruggen, A. Shahid, et al., "Ultra wideband (UWB) localization using active CIR-based fingerprinting," *IEEE Commun. Lett.*, vol. 27, no. 5, pp. 1322-1326, May. 2023.

[16] X. Guo, N. R. Elikplim, N. Ansari, et al., "Robust WiFi localization by fusing derivative fingerprints of RSS and multiple classifiers," *IEEE Trans. Ind. Inf.*, vol. 16, no. 5, pp. 3177-3186, May. 2020.

[17] C. Peng, H. Jiang and L. Qu, "Deep convolutional neural network for passive RFID tag localization via joint RSSI and PDOA fingerprint features," *IEEE Access*, vol. 9, pp. 15441-15451, Jan. 2021.

[18] X. Guo, L. Li, N. Ansari, et al., "Accurate WiFi Localization by fusing a group of fingerprints via a global fusion profile," *IEEE Trans. Veh. Technol.*, vol. 67, no. 8, pp. 7314-7325, Aug. 2018.

[19] C. Zhou, J. Liu, M. Sheng, Y. Zheng, et al., "Exploiting fingerprint correlation for fingerprint-based indoor localization: A deep learning based approach," *IEEE Trans. Veh. Technol.*, vol. 70, no. 6, pp. 5762-5774, Jun. 2021.

[20] Z. Wu, Q. Xu, J. Li, et al., "Passive indoor localization based on CSI and naive bayes classification," *IEEE Trans. Syst. Man Cybern.: Syst.*, vol. 48, no. 9, pp. 1566-1577, Sep. 2018.

[21] Y. Tao, B. Li, Z. Wang, et al., "Fingerprint-based sparse-constrained sequential sensing: Joint detection and tracking with massive antennas," *IEEE Commun. Lett.*, vol. 24, no. 4, pp. 772-776, Apr. 2020.

[22] "Ericsson Mobility Report", *Ericsson*, Jun. 2023, [Online] Available: https://www.ericsson.com/en/reports-and-papers/mobility-report/reports/june-2023

[23] L. Ni, Y. Wang, H. Tang, et al., "Accurate localizationusing LTE signaling data," in *2017 IEEE Int. Conf. CIT*, 2017, pp. 268-273.

[24] W. Fang, C. Xie and B. Ran, "An accurate and real-time commercial indoor localization system in LTE networks," *IEEE Access*, vol. 9, pp. 21167-21179, Nov. 2021.

[25] X. Ye, X. Yin, X. Cai, et al., "Neural-network-assisted UE localization using radio-channel fingerprints in LTE networks," *IEEE Access*, vol. 5, pp. 12071-12087, Jun. 2017.

[26] D. Li, X. Yang, A. Hu, et al., "LTE device radio frequency fingerprints blind extraction based on temporal-frequency domain PRACH signals," *IEEE Trans. Veh. Technol.*, vol. 72, no. 10, pp. 13229-13242, Oct. 2023.

[27] D. Li, Y. Lei and H. Zhang, "A novel outdoor positioning technique using LTE network fingerprints," *Sensors*, vol.20, no.6, pp.1691, Mar. 2020.

[28] B. Shin, J. H. Lee, C. Kim, et al., "LTE RSSI based vehicular localization system in long tunnel environment," *IEEE Trans. Ind. Inf.*, vol. 19, no. 11, pp. 11102-11114, Nov. 2023.

[29] J. He and H. C. So, "A hybrid TDOA-fingerprinting-based localization system for LTE network," *IEEE Sens. J.*, vol. 20, no. 22, pp. 13653-13665, Nov. 2020.

[30] K. Vuckovic, F. Hejazi and N. Rahnavard, "MAP-CSI: Single-site map-assisted localization using massive MIMO CSI," in *2021 IEEE Global Commun. Conf. (GLOBECOM)*, 2021, pp. 1-6.

[31] Y. Zhang, S. Zhang, R. Li, et al., "WiFi fingerprint positioning based on clustering in mobile crowdsourcing system," in *2017 12th Int. Conf. Comput. Sci. Educ. (ICCSE)*, 2017, pp. 252-256.

[32] Y. Xie, Y. Wang, A. Nallanathan, et al., "An improved K-nearest-neighbor indoor localization method based on spearman distance," *IEEE Signal Process Lett.*, vol. 23, no. 3, pp. 351-355, Mar. 2016.

[33] L. Zhang, X. Chu and M. Zhai, "Machine mearning-based integrated wireless sensing and positioning for cellular network," *IEEE Trans. Instrum. Meas.*, vol. 72, pp. 1-11, Nov. 2023.

[34] J. Hu, D. Liu, Z. Yan, et al., "Experimental analysis on weight K-nearest neighbor indoor fingerprint positioning," *IEEE Internet Things J.*, vol. 6, no. 1, pp. 891-897, Feb. 2019.

[35] C. Wu, X. Yi, W. Wang, et al., "Learning to localize: A 3D CNN approach to user positioning in massive MIMO-OFDM systems," *IEEE Trans. Wireless Commun.*, vol. 20, no. 7, pp. 4556-4570, Jul. 2021.

[36] X. Gong, A. Lu, X. Liu, et al., "Deep learning based fingerprint positioning for multi-cell massive MIMO-OFDM systems," *IEEE Trans. Veh. Technol.*, vol. 73, no. 3, pp. 3832-3849, Mar. 2024.

[37] X. Sun, C. Wu, X. Gao and G. Y. Li, "Fingerprint-based localization for massive MIMO-OFDM system with deep convolutional neural networks," *IEEE Trans. Veh. Technol.*, vol. 68, no. 11, pp. 10846-10857, Nov. 2019.

[38] X. Cui, J. Yang, J. Li, et al., "Improved genetic algorithm to optimize the Wi-Fi indoor positioning based on artificial neural network," *IEEE Access*, vol. 8, pp. 74914-74921, Apr. 2020.

[39] C. Y. Chen, A. I. C. Lai, P. Y. Wu, et al., "Optimization and evaluation of multidetector deep neural network for high-accuracy Wi-Fi fingerprint positioning," *IEEE Internet Things J.*, vol. 9, no. 16, pp. 15204-15214, Aug. 2022.

[40] J. Moon, C. Laoudias, R. Guan, et al., "Cramér-rao lower bound analysis of differential signal strength fingerprinting for crowdsourced IoT localization," *IEEE Internet Things J.*, vol. 10, no. 11, pp. 9690-9702, Jun. 2023.

[41] L. Gui, M. Yang, H. Yu, et al., "A cramér-rao lower bound of CSI-based indoor localization," *IEEE Trans. Veh. Technol.*, vol. 67, no. 3, pp. 2814-2818, Mar. 2018.

[42] Q. Jiang, F. Qiu, M. Zhou, et al., "Benefits and impact of joint metric of AOA/RSS/TOF on indoor localization error," *Appl. Sci.*, vol. 6, no. 10, pp.296, Oct. 2016.

[43] C. Yapar, R. Levie, G. Kutyniok, et al., "Real-time outdoor localization using radio maps: A deep learning approach," *IEEE Trans. Wireless Commun.*, vol. 22, no. 12, pp. 9703-9717, Dec. 2023.

[44] 3GPP, "Evolved universal terrestrial radio access (E-UTRA); User equipment (UE) radio transmission and reception," 3GPP TS 36.101, Release 8, 2021.

[45] S. Kimia and Z. M. Kassas, "LTE receiver design and multipath analysis for navigation in urban environments," *Navigation*, vol. 65, no. 4, pp.655-675, Dec. 2018.

[46] 3GPP, "Evolved universal terrestrial radio access (E-UTRA); Requirements for support of radio resource management," 3GPP TS 36.133, v16.8.0, 2021.

[47] C. Laoudias, A. Moreira, S. Kim, et al., "A Survey of enabling technologies for network localization, tracking, and navigation," *IEEE Commun. Surv. Tutorials*, vol. 20, no. 4, pp. 3607-3644, Jul. 2018.

[48] J. Fan, J. Zhang and X. Dou, "Single-site indoor fingerprint localization based on MIMO-CSI," *China Commun.*, vol. 18, no. 8, pp. 199-208, Aug. 2021.

[49] S. Han, C. Zhao, W. Meng, et al., "Cosine similarity based fingerprinting algorithm in WLAN indoor positioning against device diversity," in *2015 IEEE Int. Conf. Commun. (ICC)*, 2015, pp. 2710-2714.

[50] O. Pele and M. Werman, "Robust real-time pattern matching using bayesian sequential hypothesis testing," *IEEE Trans. Pattern Anal. Mach. Intell.*, vol. 30, no. 8, pp. 1427-1443, Aug. 2008.

[51] C. Schaffer, "Selecting a classification method by cross-validation", *Mach. Learn.*, vol. 13, no. 1, pp. 135-143, Oct. 1993.

[52] A. Alkhateeb, "DeepMIMO: A generic deep learning dataset for millimeter wave and massive MIMO applications," in *Proc. of The Information Theory and Applications Workshop (ITA)*, 2019, pp. 1-8.

Zhinan Hu received the B.Eng. degree from Xiamen University, Xiamen, China, in 2017, and the master's degree in information and communication engineering from Xi'an Jiaotong University, Xi'an, China, in 2020. She is currently pursuing a Ph.D. degree at the School of Electronic Information and Electrical Engineering, Shanghai Jiao Tong University. Her research interests include massive MIMO wireless communications, signal processing for wireless communications, and wireless localization.

Xin Chen (M'15-SM'20) received the PhD degree in electronic and communication system from Politecnico di Torino, Italy. He is an Associate Professor at the School of Electronic Information and Electrical Engineering, Shanghai Jiao Tong University, China. His research topic covers multipath channel modeling and mitigation, interference detection and localization, and software receiver design.

Zhenyu Zhou (Senior Member, IEEE) received the M.E. and Ph.D. degrees in international information and communication studies from Waseda University, Tokyo, Japan, in 2008 and 2011, respectively. From September 2012 to April 2019, he was an Associate Professor with the School of Electrical and Electronic Engineering, North China Electric Power University, Beijing, China, where he has been a Full Professor since April 2019. His research interests include power internet of things, smart grid information and communication, communication-sensing-computing integration, and smart grid energy management. He was the recipient of the IET Premium Award in 2017, IEEE Globecom 2018 Best Paper Award, IEEE International Wireless Communications and Mobile Computing Conference 2019 Best Paper Award, and IEEE Communications Society Asia-Pacific Board Outstanding Young Researcher. He was an Associate Editor for IEEE INTERNET OF THINGS JOURNAL, IET Quantum Communication, IEEE ACCESS, and EURASIP Journal on Wireless Communications and Networking, and the Guest Editor of IEEE Communications Magazine, IEEE TRANSACTIONS ON INDUSTRIAL INFORMATICS, and Transactions on Emerging Telecommunications Technologies. He is an IET Fellow and a Senior Member of the Chinese Institute of Electronics and the China Institute of Communications.

Shahid Mumtaz is an IET Fellow, IEEE ComSoc and ACM Distinguished Speaker, recipient of IEEE ComSoc Young Researcher Award (2020), founder and EiC of the IET Journal of Quantum Communication, ViceChair of the Europe/Africa RegionIEEE Com Soc Green Communications Computing Society, and Vice-Chair of IEEE Standard P1932.1: Standard for Licensed/Unlicensed Spectrum Interoperability in Wireless Mobile Networks. He is the author of 4 technical books, 12 book chapters, 300+ technical papers (200+ IEEE journals/transactions, 100+ conference proceedings), and received 2 IEEE best paper awards in the area of mobile communications. Most of his publication is in the field of wireless communication. He is serving as Scientific Expert and Evaluator for various research funding agencies. He was awarded an Alain Bensoussan Fellowship in 2012. He was the recipient of the NSFC Researcher Fund for Young Scientist in 2017 from China.